



City Research Online

City, University of London Institutional Repository

Citation: Kouris, L.A.S., Meireles, H., Bento, R. and Kappos, A. J. (2014). Simple and complex modelling of timber-framed masonry walls in Pombalino buildings. *Bulletin of Earthquake Engineering*, 12(4), pp. 1777-1803. doi: 10.1007/s10518-014-9586-0

This is the accepted version of the paper.

This version of the publication may differ from the final published version.

Permanent repository link: <https://openaccess.city.ac.uk/id/eprint/4792/>

Link to published version: <http://dx.doi.org/10.1007/s10518-014-9586-0>

Copyright: City Research Online aims to make research outputs of City, University of London available to a wider audience. Copyright and Moral Rights remain with the author(s) and/or copyright holders. URLs from City Research Online may be freely distributed and linked to.

Reuse: Copies of full items can be used for personal research or study, educational, or not-for-profit purposes without prior permission or charge. Provided that the authors, title and full bibliographic details are credited, a hyperlink and/or URL is given for the original metadata page and the content is not changed in any way.

Simple and complex modelling of timber-framed masonry walls in Pombalino buildings

L.A.S. Kouris¹, H. Meireles², R. Bento², A.J. Kappos^{1,3}

Abstract

Timber-framed masonry has been developed as an effective lateral-load resisting system in regions of high seismicity such as Southern Europe. A salient feature of the 'last generation' of timber-framed (TF) buildings is the presence of diagonal members that may consist of two diagonal braces. The present study focusses on alternative modelling procedures, ranging from simple to rather complex, for this interesting type of traditional structure. All models are applied to study the behaviour of full-scale specimens of diagonally-braced TF panels. The complex model is based on plasticity with contact surfaces for the connection between timber diagonals and masonry infills. A parametric analysis using this model shows that masonry infills affect only slightly the lateral force carried by this TF panel configuration. Furthermore, two simple modelling techniques are put forward for application in the analysis of large, realistic structures incorporating TF walls. The first one is directly connected to the complex modelling and is based on substructuring. A nine-step procedure is developed and is found to properly reproduce the response of the test specimens. The second simple model is a phenomenological one, developed on the basis of observed behaviour during tests and is a complete hysteretic model; however, for comparison purposes, all models are evaluated here with respect to the prediction of the envelope (pushover) curve for the walls tested under lateral loads.

Keywords: *timber-framed masonry, non-linear static analysis, pushover curve, microscopic modelling, macroscopic modelling.*

¹Department of Civil Engineering, Aristotle University of Thessaloniki, Greece

²ICIST, Instituto Superior Técnico, Technical University of Lisbon, Lisbon, Portugal

³Department of Civil Engineering, City University London, UK; e-mail:Andreas.Kappos.1@city.ac.uk

1. Introduction

1.1. General

For thousands of years traditional structures were built in mainly four materials. These were earth (from which bricks come from, for instance), stone, wood, and natural plant fibres. Using these four elements impressive structures were built, some of which are still standing today.

For example, in Lisbon, Portugal, *Pre-Pombalino* (pre-1755) buildings, *Pombalino* buildings (1755-1870), *Gaioleiro* buildings (1880-1990) and to some extent *Placa* buildings (1940-1960) were built using such materials. Some of these buildings are more than 250 years old, and are still used, mainly for housing. In these buildings, masonry (constructed with the available stone material and lime mortar) was used mainly for the exterior walls (façades and gable walls), while wood was used for the roof and floors.

As unreinforced masonry suffers from both low tensile strength and low ductility, strengthening of masonry structures by means of wood elements was introduced in Portugal after the 1755 Lisbon earthquake. In fact, this type of reinforcement dates far back in time, even the Bronze Age in Greece, and the early Roman Times (Kouris and Kappos, 2012; Kouris 2012).

This type of construction, known as timber-framed (TF) masonry, can be found around the world with several different configurations, all with timber-framed masonry panels in the exterior and/or interior walls of the building. TF masonry generally consists of masonry walls reinforced with timber elements, including horizontal, vertical elements, and diagonal braces.

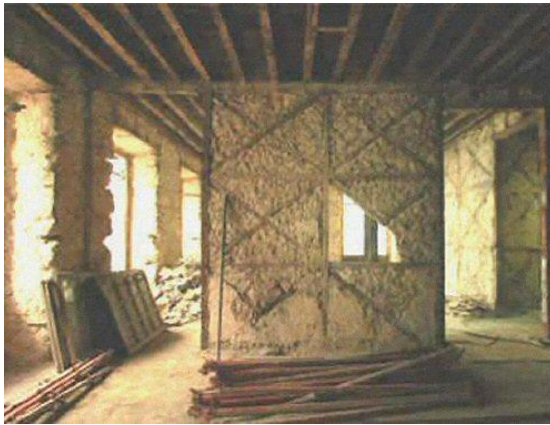
1.2. The *Pombalino* construction

The mixed wood-masonry XVIII century *Pombalino* buildings of downtown Lisbon have a recognized patrimonial value both nationally and internationally. They were introduced after the 1755 catastrophic earthquake as a structural solution that would provide the required seismic resistance. Based on the know-how of that time and on the empirical knowledge gathered from the buildings that survived the earthquake a new construction type was proposed, this being generally referred to as *Pombalino* construction nowadays. The buildings were designed with a three-dimensional wood truss that provides resistance to horizontal forces in any direction. The wood truss, called *Gaiola* (cage), is a characteristic of these buildings, and was widely used during the reconstruction of Lisbon. It was arguably the first case in history of an entire town built with the purpose of providing seismic resistance to its buildings.

This construction type can be summarized as follows (for more detailed descriptions see Mascarenhas 2005; Cardoso et al. 2005): Buildings were built in quarters, each block comprising an average of 10 buildings. The foundation system was ingenious, consisting of a system of wooden piles over the alluvium layers. The piles are similar and repetitive, on average 15 cm in diameter and 1.5 m in length. These form two parallel rows in the direction of the main walls, which were linked at the top by horizontal cross-members attached by thick iron nails.

The construction between the ground and first floors consisted of solid walls and piers linked by a system of arches. In more elaborate cases, thick-groined vaults spanned between the arches, which protected the upper floors from the spread of any fire that might start at ground floor level.

From the first floor up this building system has the aforementioned three-dimensional timber Gaiola structure, thought to be an improved system based on prior traditional wooden houses. Gaiola is composed of traditional timber floors and new mixed timber-framed masonry panels (“frontal” walls) that would support not only the vertical loads but also horizontal seismic loading. These TF walls are one of the key characteristics of these buildings, and a paradigm of the abovementioned TF masonry structures. They are made up of a wooden truss system with X-type diagonal braces, filled with a weak mortar masonry in the empty spaces. Figure 1b shows these walls with no masonry fillings yet. It is important to point out also that, based on recent studies (e.g. Meireles, 2012; Meireles et al., 2012), these walls would have a beneficial effect on the out-of-plane failure of the façade walls since they were connected to them through the floor.



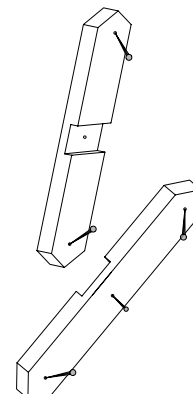
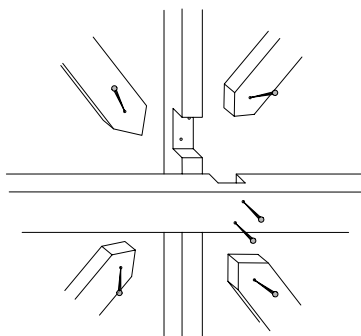
(a)



(b)

Figure 1 A “Pombalino” building: a) Interior view of; b) “Frontal” panel inside the building.

Figure 2 shows typical connections of TF wall timber members. It can be seen that the vertical and horizontal members are cut (grooved) at their mid-sections for them to be connected. In Figure 2b one can see how two diagonal elements are attached together; these are also grooved at half their thickness to be attached to each other.



(a)

(b)

Figure 2 Details of timber connections: (a) Members framing into a middle central connection; (b) diagonal elements. [Meireles, 2012]

1.3. Overview of existing models

Modelling of these challenging structures has received little attention in the past. Depending on the scope of the analysis different approaches are in order. For instance, if a single wall or panel is analysed, sophisticated models accounting for material and boundary condition nonlinearity can be used; e.g. Kouris & Kappos (2012) focused more on the nonlinear response of the timber braces, while Doudoumis (2010) focussed on the varying boundary conditions, i.e. the separation of the masonry infill from the surrounding timber frame. On the other hand, if entire actual buildings are studied, more macroscopic approaches have to be adopted, and nonlinearities can be treated in a more indirect or approximate way; e.g. Cardoso et al. (2005) have analysed an actual Pombalino building using a series of elastic analyses, wherein members that were predicted to fail were removed from the model and elastic analysis was resumed. Whether a model is complex or simple, a prerequisite is that it should capture at least the salient features of the structure studied, and this can only be assessed if prediction of experimentally observed behaviour is attempted. This paper presents for the first time a comparative assessment of available simple and complex models for nonlinear static (pushover) analysis of timber-framed masonry walls, carried out in the light of available experimental results. In this respect, its findings could assist the analyst in selecting proper models, taking into account the size of the problem at hand. Moreover, some of the existing models are extended here to increase their range of applicability.

2. Overview of tests on TF masonry walls of Pombalino buildings

2.1. Tests at IST

Very few tests on TF masonry walls are available in the literature. Tests on three identical TF walls under static horizontal cyclic loading with imposed displacements were carried out at the laboratory of IST (Instituto Superior Técnico), Lisbon (Meireles et al. 2012); only the results provided by the last two tests were taken into account here since the first test had a different failure mode which does not occur in real Pombalino walls. The walls had 4 crossed braces in an arrangement of 2x2 modules (each module comprising one cross brace). They were 2.6x2.64 m² in height and length, respectively. The masonry infill consisted of hydraulic lime with layers of broken bricks or tiles, in an attempt to reproduce what exists in actual *Pombalino* buildings. The amount of vertical loading, applied by steel rods and 4 hydraulic jacks, was based assuming that the wall was situated at the first storey. The nails used (Figure 3 and Figure 4) were all pyramidal, 12.5 cm long and a section of 10x6 mm² at the base.

Exceptionally, the nails used to connect the diagonals to each other are smaller, of 7.5 cm in length with a base section of 5x5 mm². The layout of the setup, in the laboratory, can be seen in Fig. 5.



Figure 3 Nailed connections: a) central nodes; b) corner nodes.

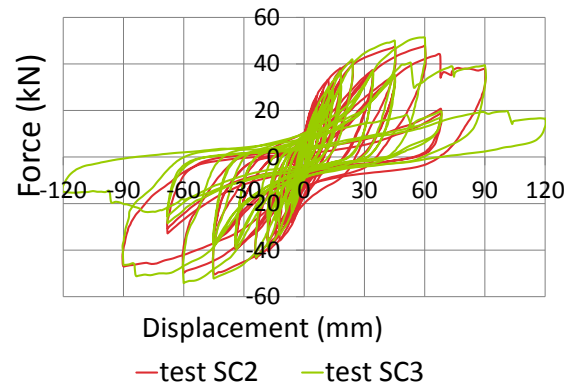


Figure 4 Nails used in the experimental testing at IST.

The loading protocol used was that of CUREE (Krawinkler et al. 2000) for ordinary ground motions, tailored specifically to wood structural components. In Figure 5a one can see the load cell on the left to measure forces and the linear variable displacement transducer (LVDT) on the right to measure displacements at the top. Figure 5a also indicates that the wall is fixed to the yellow horizontal reaction beam by the lower wood horizontal beam through omega shaped plates. The hysteretic behaviour of the TF walls subjected to cyclic loading is shown in Figure 5b. More information about the test and its results can be found in Meireles et al. (2012), Meireles (2012).



(a)



(b)

Figure 5 IST tests: a) Final layout of the experiment with load cell, LVDT and jacks (2x2 panel); b) recorded hysteresis loops.

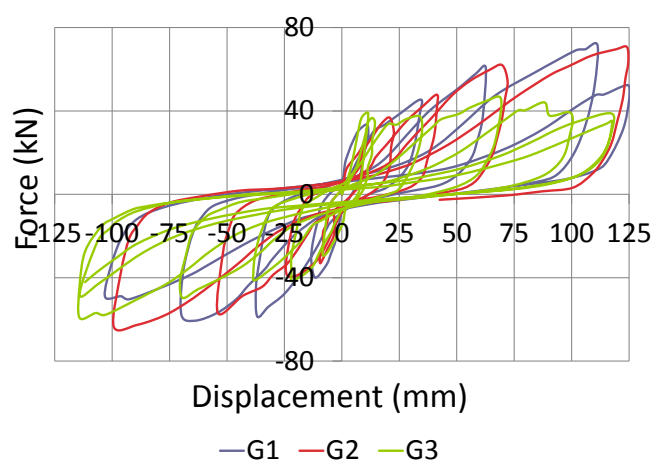
2.2. Tests at LNEC

Another experimental test (Santos 1997) was performed back in 1997 at LNEC (Portuguese National Laboratory for Civil Engineering), on specimens extracted from an actual Pombalino building in downtown Lisbon. Three TF walls (G1, G2 and G3) were tested under static horizontal cyclic loading with imposed displacements. Nevertheless, in this case, no specific loading protocol was used and no vertical loading was applied. More details of the tests are found in Santos (1997) and Meireles (2012). Figure 6a is a photograph of one of the walls (G2) at the end of the test, while Figure 6b summarises the results of all tests.

It is noted that specimens G1, G2 and G3 tested at LNEC were all 3x1 panel modules, while those tested at IST were 2x2 modules.



(a)



(b)

Figure 6 LNEC tests: a) Wall G2 while being tested; b) test results (Santos 1997).

3. Microscopic modelling

A previously developed micro - model based on a Hill-type plasticity law (Kouris and Kappos 2012) is extended and evaluated here in the light of the aforementioned experimental results. Hence the model is applied to both specimens from a building subjected to the decaying action of the long-time exposure to the environment, as well as to specimens with new materials fabricated in the laboratory. It is noted that this rather complex model can be applied to virtually any structural configuration, since it does not involve phenomenologically derived empirical coefficients.

3.1. Overview of existing model

A detailed description of the original model can be found in Kouris and Kappos (2012) and Kouris (2012); its basic features are:

- Gradual stiffness degradation in timber elements is modelled using a Hill-type yield criterion (Hill 1948; Shih and Lee 1978). The plasticity model adopted herein considers wood as a material with isotropic expansion of its yield surface, which under axial compressive load responds following a trilinear stress-strain curve; the second branch has a slope $0.1E$ (E is the modulus of elasticity of wood) while the third branch is horizontal (plastic behaviour).
- The well-known (especially for old structures) inadequate connection between the wooden braces and the surrounding frame is modelled using a cohesionless contact model based on the Mohr-Coulomb friction law. Hence the braces can separate from, and/or slide along, the wooden frame and at their junction.

It is seen that the nonlinearities accounted for in this model are related to the wooden members and their connections. Masonry is assumed to disconnect from the surrounding frame at an early stage and does not contribute substantially to the lateral load resistance of the TF panel. This is a reasonable assumption for X-braced frames, but in other configurations with less effective bracing, the masonry infill can play a more significant role. Hence, the model is extended here, to account also for nonlinear behaviour of the masonry infill.

3.2. Extensions of the model

3.2.1. Plasticity model for masonry

Masonry, which is a non-homogenous, anisotropic and discontinuous (as soon as it cracks) quasi-brittle material, does not actually present a yielding behaviour such as that implied by plasticity theory. However, if masonry is treated macroscopically, a plastic-like behaviour can be determined with yielding, hardening, and finally failure, accounting for all cracks observed at a meso-scale. Regarding the yield criterion, simple ones have been used, such as the Drucker-Prager one (Addessi et al. 2002; Pallarés et al. 2008) or others more specific to masonry materials (Lourenco 2000; Syrmakezis and Asteris 2001). For plane stress conditions ($\sigma_3 = \sigma_{23} = \sigma_{13} = 0$) and for principal stresses, the Drucker-Prager (1952) yield criterion can be simplified to

$$a \frac{\sigma_1 + \sigma_2}{3} + \sqrt{(\sigma_1^2 - \sigma_1 \sigma_2 + \sigma_2^2)} - \sigma_Y(\hat{\epsilon}_{pl}) = 0 \quad (1)$$

where σ_Y is the width of the Drucker-Prager surface and α a coefficient of the masonry material. Rearranging terms in the above Equation, the criterion can be expressed as an ellipse with inclined axes (**Figure 7**):

$$\left(1 - \frac{a^2}{9}\right)(\sigma_1^2 + \sigma_2^2) - \left(1 + \frac{2a^2}{9}\right)\sigma_1\sigma_2 - \sigma_Y^2(\hat{\epsilon}_{pl}) = 0 \quad (2)$$

Equation (2) for $\sigma_1 = 0$ and $\sigma_2 = f_m$ (the compressive strength of masonry) and for $\sigma_1 = \sigma_2 = \beta f_m$ (β being a fraction of uniaxial strength) results in a system of linear equations, from which α and σ_Y can be calculated. A comparison of the Drucker-Prager criterion against the well-known experimental results by Page (1981) on biaxial stress of masonry wallets is illustrated in Figure 7 (for $\sigma_Y = -1$ MPa, $\alpha = 1.34$). These and other comparisons clearly show that the Drucker-Prager criterion cannot be simultaneously accurate in all four regions in the stress space (i.e. in compression (-,-), tension (+,+), compression-tension (-,+) and tension-compression (+,-)). Depending in which region is the most important for the problem at hand, the criterion could be tailored accordingly.

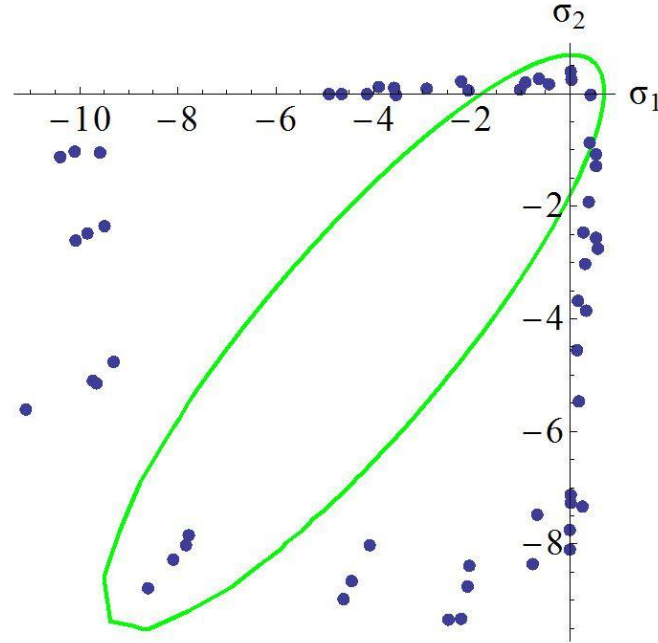


Figure 7 Drucker-Prager criterion against experimental results for biaxial stress.

A better simulation of the biaxial masonry behaviour is achieved by the power-law form of the Drucker-Prager criterion, which for plane stress conditions is given by:

$$a \frac{\sigma_1 + \sigma_2}{3} + \sqrt{\left(\sigma_1^2 - \sigma_1 \sigma_2 + \sigma_2^2\right)^b} - \sigma_Y^b(\hat{\varepsilon}_{pl}) = 0 \quad (3)$$

where $\hat{\varepsilon}_{pl}$ is the mean plastic strain. It is noted that two terms of the Drucker-Prager criterion have an exponent b . Obviously, for $b = 1$ Equation (3) results in the classical Drucker-Prager criterion of Equation (1). The favourable effect of the index b in the Drucker-Prager criterion appears from two applications in Figure 8 (drawn for $\sigma_Y = 3.33$ MPa, $\alpha = 4$, $b = 1.57$). Parameter σ_Y increases the width of the secondary axis of the ellipse and the coefficient α displaces the centre of the ellipse downwards along the inclined axis. The coefficient b increases the width of the primary axis and hence a better fit to the experimental data can be achieved. It can be seen that the modified Drucker-Prager criterion captures well the compression area of the stress space but rather poorly the tension-compression area.

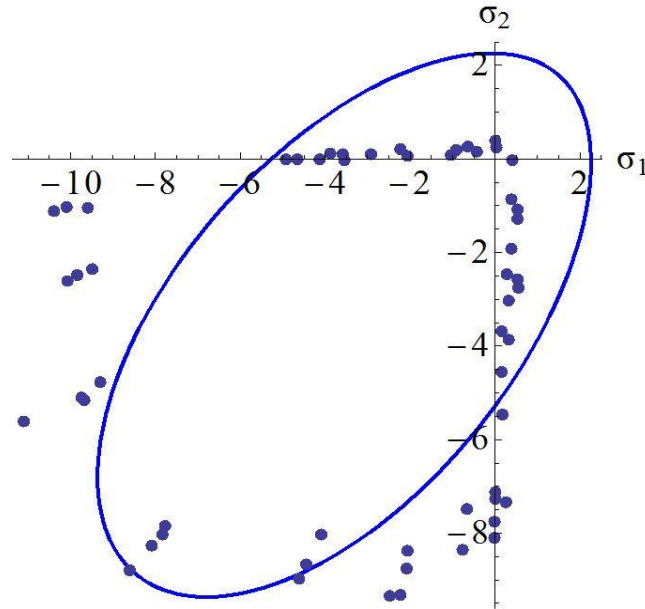


Figure 8 Modified Drucker-Prager law against experimental results for biaxial stress

Like most other materials, masonry undergoes work hardening i.e. increase in the yield stress with increasing strain. Among the different empirical expressions that have been proposed for the hardening of masonry, an elliptical hardening equation originally derived for concrete is adopted herein:

$$\sigma(k) = \sigma(\varepsilon_{eq}^p) = \sigma_o + (f_m - \sigma_o) \sqrt{1 - \left(\frac{\varepsilon_{eq,t}^p - \varepsilon_{eq}^p}{\varepsilon_{eq,t}^p} \right)^2} \quad (4)$$

In Equation (4) f_m is the mean compressive strength of masonry, σ_o corresponds to the 'yield' stress (i.e. the initiation of plastic non-reversible strain) taken equal to one third of the uniaxial strength, and $\varepsilon_{eq,t}^p$ is the equivalent plastic strain at maximum compressive stress, assumed

equal to 8×10^{-4} (Lourenc o et al. 1997). With these values the hardening law (in terms of plastic stresses) is illustrated in Figure 9.

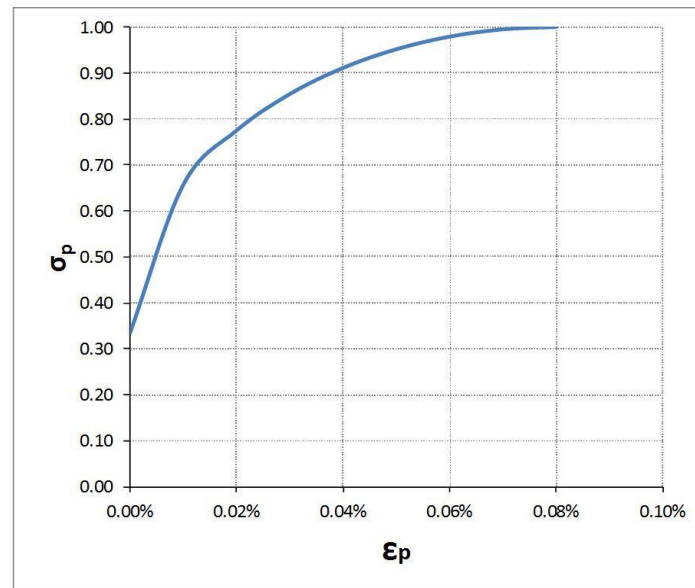


Figure 9 Hardening law in terms of plastic stresses.

3.2.2. Parametric investigation on the friction coefficient

It is first noted that in actual old buildings the diagonal braces are usually unable to provide any noticeable resistance to tension; hence, in the present model any such resistance is neglected while compression forces are accounted for by friction connection between the brace and the surrounding timber frame. In order to quantify the influence of the friction coefficient μ_f between the frame and the diagonals, a parametric analysis was carried out and the model was implemented in ANSYS (2011). As a sensitivity analysis, five different friction coefficients were considered, varying from zero up to full connection; the intermediate values that have been used in several analytical models (Doudoumis 2010; Parisi and Piazza 2000; Patton-Mallory et al. 1997) were $\mu_f = 0.1, 0.4, 0.5$, while 0.6 and 1.0 apply for the (unrealistic) case of increased friction around the metal nails, to investigate the transition from relative sliding to full connection. It is noted that the static and the dynamic coefficients are assumed to coincide. For this sensitivity analysis a TF wall was considered with standard dimensions 2.0x1.7 m (Figure 10). The mechanical properties of the materials are presented in Table 1 (elastic properties) and Table 2 (inelastic properties) and correspond to pine wood usually used in these structures as well as in the experimental investigation (§2.1 and 3.3). Vertical loading was also considered; axial loading in both timber posts is equal to 4.25 kN and uniformly distributed load on the beam is equal to 0.5 kN/m (plus the self-weight of the materials) which correspond to the vertical load applied in the tests (§2.1). For timber the plastic behaviour is described by the Hill yield criterion and for masonry by the modified Drucker-Prager yield criterion which better captures the compression area since masonry is mainly stressed in compression and shear due to the

friction forces (§3.2.1). Nevertheless, it will be seen that the state of stress in masonry infills is far from their yield locus.

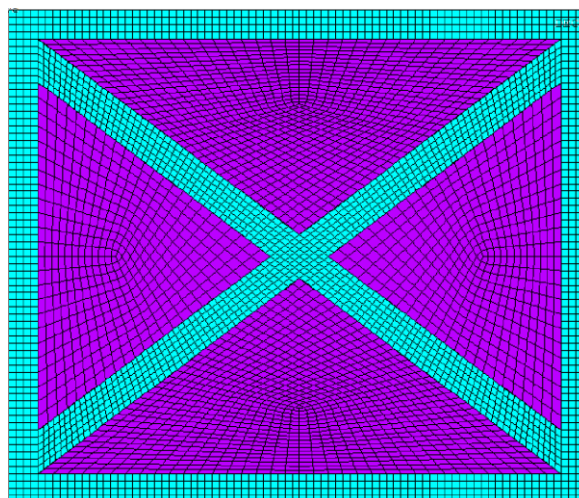
Table 1. Elastic properties of materials of TF wall (in GPa).

Element	Modulus of Elasticity E_x	Modulus of Elasticity E_y	Shear Modulus G
Masonry	1.5		0.63
Timber	11	0.37	0.69

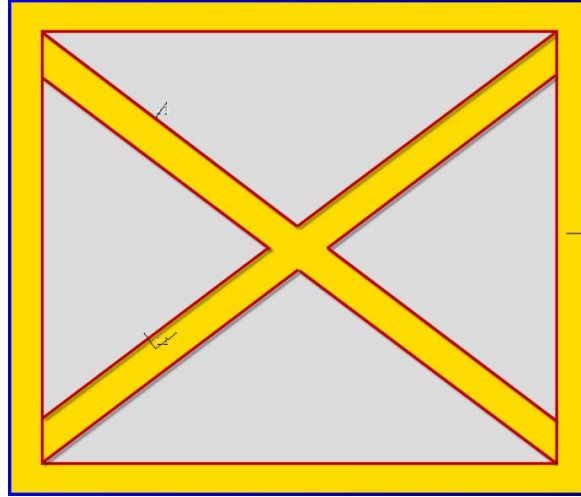
Table 2. Material strengths (in MPa).

Element	Compressive strength $f_{c,x}^a$	Compressive strength $f_{c,y}^a$	Tensile strength $f_{t,x}^a$	Tensile strength $f_{t,y}^a$
Masonry	1.5		0.15	
Timber	23.1	5.8	15.4	0.4

^a x, y denote the directions parallel and perpendicular to the fibres, respectively.



(a)



(b)

Figure 10 TF panel with masonry infills: (a) simulation with FE (in light blue timber elements and in magenta masonry elements) and (b) the contact surfaces in solid red lines.

Plastic stresses for the TF walls without infills are displayed in Figure 11 where it is seen that significant plastic stresses have developed only at the extremities of the diagonal in compression, and some in the connection of timber braces and posts. A similar trend is noted in Figure 12 (case $\mu_f = 0.5$) where for the TF wall with masonry infills not connected to the surrounding timber frame, concentration of maximum stresses occurs in the edges of the diagonals. In this TF wall, masonry infills are not substantially loaded; in fact, they remain almost intact, as expected since the discontinuities transmit only shear stress and some compression. The main stress path of the compressive stresses resulting from horizontal loading is obviously through the diagonals.

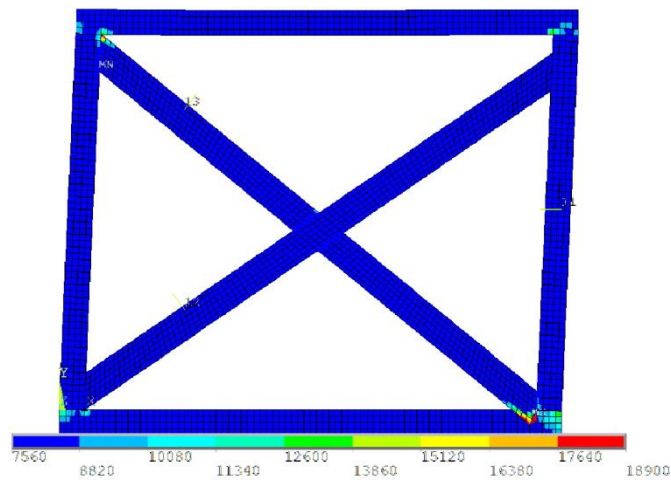
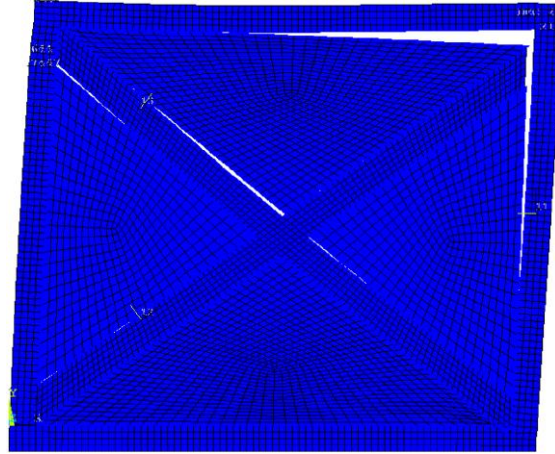
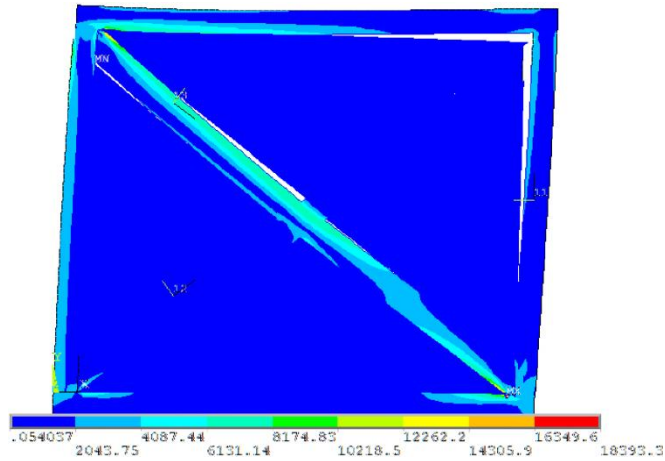


Figure 11 Plastic stresses for the 'bare' TF wall in kPa.



(a)



(b)

Figure 12 TF walls horizontally loaded: (a) deformed shape and (b) stress field (in kPa) at the final step of the nonlinear analysis.

A different performance is observed for the TF wall with full connections of the diagonals, the frame and the masonry infills as displayed in Figure 13. In this case the wall sustains much higher loads. A substantial part of the timber frame and the diagonals has reached its maximum strength ($\sigma/f_m = 1$). Plastic stresses have also been spread over a small part of masonry infills. It should be recalled here that such full connections barely ever exist in actual buildings.

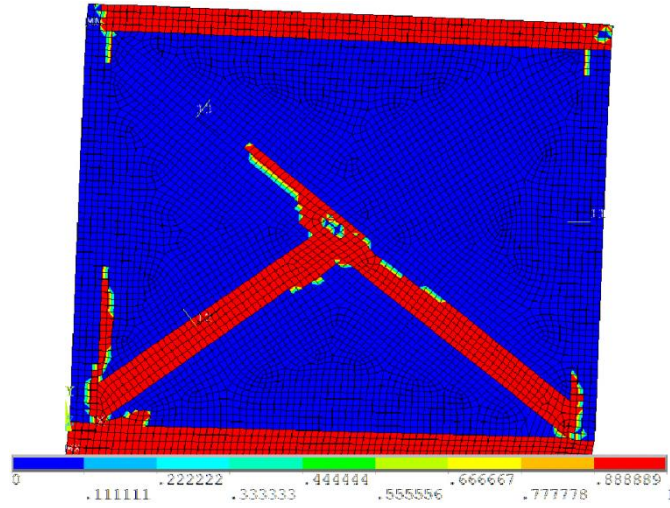


Figure 13 TF wall with full connections of masonry infills: stress ratios (σ/f_m).

Pushover curves for the examined TF walls are presented in Figure 14, where the walls reach the ultimate state before any numerical instability due to excessive plastic strain. TF wall with masonry infills in full contact with the surrounding frame exhibits about twice the stiffness of all other cases (2.08 on average). This should be mainly attributed to the contribution of the diagonal in tension to the lateral resistance rather than to the masonry infills themselves. The stiffness of the bare frame does not substantially differ (less than 10%) from that of TF walls with discontinuities. This is in line with the expected performance since the discontinuities allow relative sliding. Note that the experimental results indicate an early separation and relative sliding and detachment of the masonry infills. Differences in the initial elastic stiffness among the TF walls having various friction coefficients μ_f do not exceed 6% but the effective stiffnesses at yielding (i.e. F_y/δ_y) differ only 3%. Regarding maximum displacements, there is a gradual decrease of the displacement capacity with increasing friction coefficient, though considerably notable only for the TF wall with full contact. Moreover, its maximum base shear is much higher (on average 94%) than the maximum base shears in the other TF walls. Finally, parametric analysis shows that a global friction coefficient $\mu_f = 0.1$ to 0.4 around timber and masonry surfaces is matching very well both in terms of ductility and stiffness with the friction coefficient $\mu_f = 0.5$ when masonry infills are neglected.

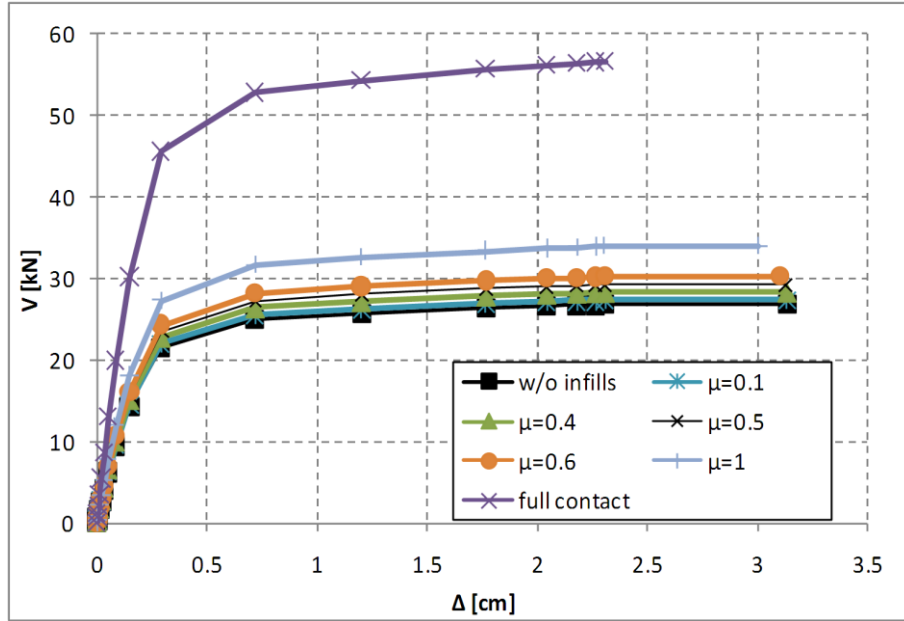


Figure 14 Pushover curves of TF walls with various friction coefficients.

In a nutshell, the experimental and analytical results show that in a TF wall with two diagonal braces early separation of the diagonal in tension occurs, as well as relative sliding of the masonry infills with respect to the timber frame. This behaviour can be more accurately simulated by introducing discontinuities, whereas the assumption of full contact does not reflect the actual response. Differences among masonry-infilled walls with various friction coefficients and the bare TF wall are not significant and imply that a bare TF wall with diagonals activated only in compression with a friction coefficient $\mu=0.5$ can provide a good approximation of the actual behaviour.

3.3. Verification using experimental data

The model is used for the nonlinear (NL) static analysis of the specimens tested at IST. The geometry of the specimens that consist of four TF panels is given in section 2 and in more detail in Meireles (2012). Maritime pine (*Pinus pinaster*, Ait), used in the specimens, is a species of wood found widely in South-western Europe whose mechanical characteristics vary from one region to the next. Studies on Portuguese *Pinus pinaster* specimens gave a range of mechanical characteristics; values of the compressive strength in the direction of the fibres varied from $f_{c,0,k}^{min} = 18$ MPa to $f_{c,0,k}^{max} = 25$ MPa (Cruz et al. 1998). The compressive strength of *Pinus Pinaster* Pinho Bravo in the direction perpendicular to the fibres varies from $f_{c,90,k}^{min} = 6.9$ MPa to $f_{c,90,k}^{max} = 7.3$ MPa. The modulus of elasticity in the direction of the fibres varies from $E_{0,mean}^{min} = 12$ GPa to $E_{0,mean}^{max} = 14$ GPa and perpendicular to the fibres from $E_{90,mean}^{min} = 4$ GPa to $E_{90,mean}^{max} = 4.6$ GPa. Analysis using the model illustrated in Figure 15 is therefore performed for ten different material property sets, bounded by the aforementioned limits. In Figure 16 the lateral capacity (pushover) curve of the detailed model using the varying wood mechanical

characteristics are plotted against the envelope curves of IST. In bold solid line are plotted the average values from the entire set of analyses; this curve is mirrored also in the negative values range. It is seen that the application of the micro - model to the IST specimens provides a good match. Similarly satisfactory results, using the same model, were found by Kouris & Kappos (2012) and will not be repeated here, for the economy of the paper.

The response of the ten models with varied mechanical properties for wood shows that maximum base shear increases, almost proportionally, with increasing wood strength. The mean maximum base shear from the analyses is 42.6 kN, with a coefficient of variation 16%. Compared to the experimentally derived strengths, the analytical model is more conservative as the mean analytical value of peak base shear is 15% lower than the experimental one. Nevertheless, the difference of the analytical estimation using "maximum" properties is higher than the mean experimental one and within the standard deviation range. Specimen SC1 is the only one to have maximum base shear lower in one direction than the average analytical one.

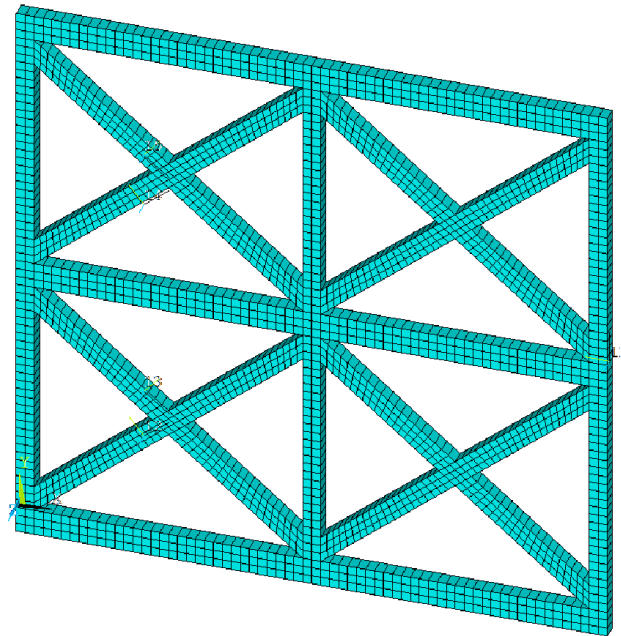


Figure 15 Simulation of the TF specimens of the LERM laboratory.

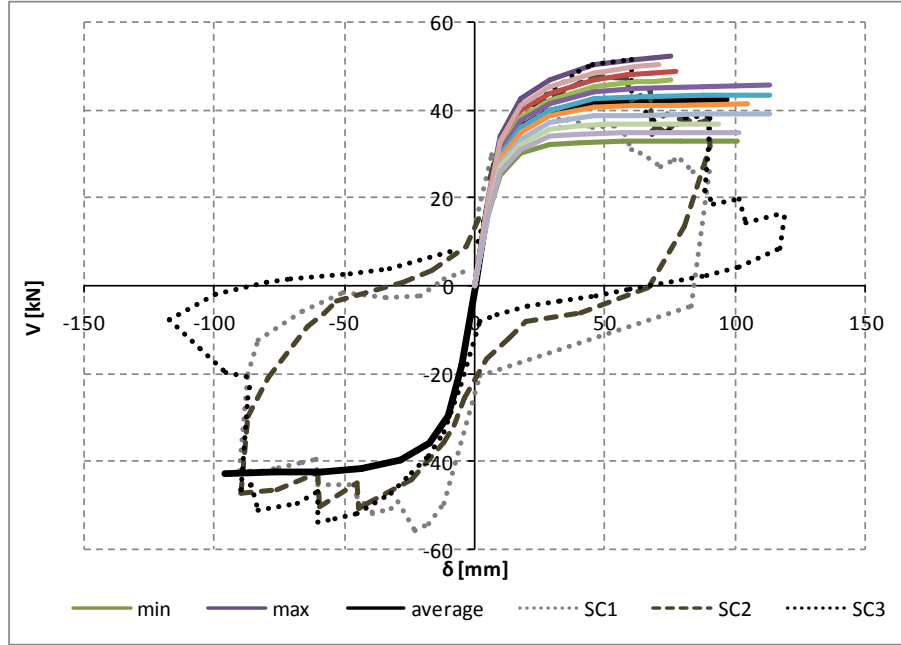


Figure 16 Comparison of the detailed model (solid line) against IST specimens (dotted lines).

With regard to displacements, comparison between test and analysis shows a good match. The difference of the maximum displacement predicted by the analytical model from the average maximum experimental one is only 3%. However, individual differences up to 19 % are found, but this concerns only one specimen, for a cycle with substantially degraded base shear. It is noted that prediction of displacements is even more important than that of base shears as they control the ductility and energy dissipation capacity under reversed cyclic loading. Of course, particular care must be taken in analytically predicting ultimate displacements, since, as is evident from Figure 16 microscopic analysis cannot capture strength degradation and is terminated when it fails to converge.

Another interesting feature is the degree of penetration of the diagonals braces into the surrounding frame, a feature that can only be captured by such a sophisticated analysis. Penetration is found to reach up to 1 mm for the lower left panel. Moreover the sliding of the diagonals in compression has a maximum value 0.25 mm for the same diagonal (Figure 17). It is interesting to note that due to excessive local plastic strain at the ultimate state of the diagonal at the bottom right corner of the TF wall, the penetration and relative sliding due to friction phenomena appears to be very small. Other critical results are the compressive stress between the sliding interfaces with a maximum value reaching about 10 MPa. It is clear that strongly localised quantities can result from this refined analysis, offering a very detailed picture of the state of the frame at various loading stages. Having said this, experimental results for fully verifying such local quantities are generally not available; in a quantitative sense, though, values of the predicted penetration of the braces were in line with observed behaviour of the IST specimens.

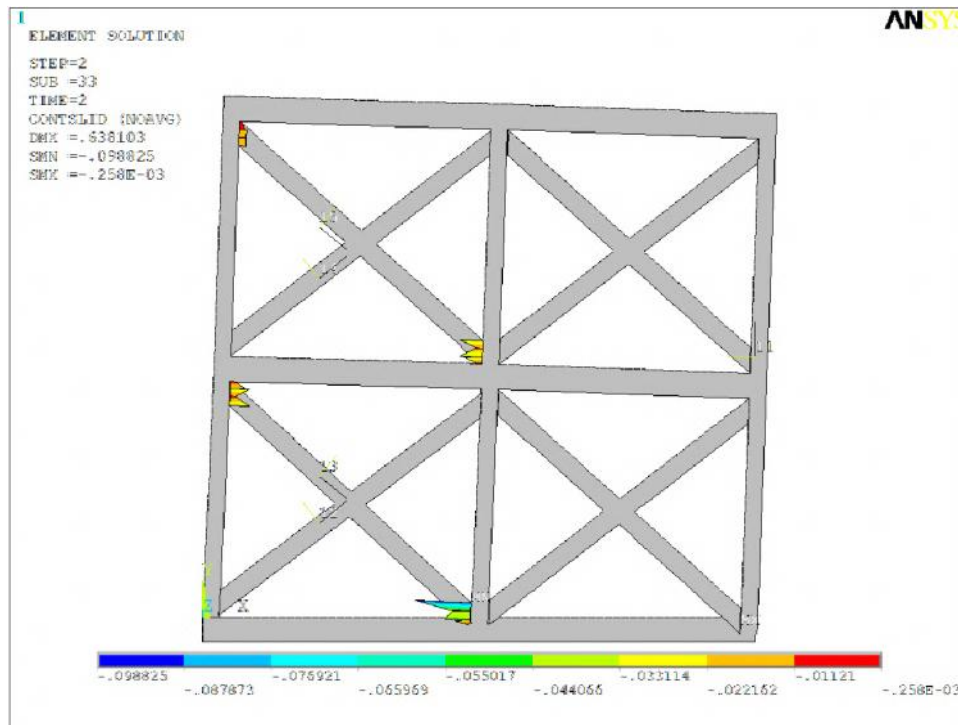


Figure 17 Sliding of the diagonals (in mm).

4. Macroscopic modelling

4.1. Simple model with beam-column elements

Notwithstanding the fact that the complex model of section 3 can give detailed and generally reliable results, the computational effort to analyse actual buildings is a major drawback that limits its applicability. For this reason a simple model has been developed using the familiar beam-column elements and NL axial hinges on the diagonals to accommodate all plastic deformation developing in TF walls (Kouris and Kappos 2012). This model is further verified here using the new experimental results. A modification to the existing model introduced herein is the different procedure for calculating the vertical loading in the posts. In the original model the vertical loads that were included in the TF wall were extracted from the last step of the analysis. In this way, they reflected not only the vertical load applied during the tests, but also the axial loads in the vertical posts to balance the overturning moment at the final state of the TF wall. However, this presents two drawbacks: (i) the vertical loads are calculated using elastic models, (ii) the final base shear should be known a priori. For a TF wall with a limited number of panels these drawbacks can be overcome with some iterative analyses, whereas for an entire real building this iterative procedure is hardly feasible. However, in view of the cyclic nature of the seismic loads a rather simple and practical estimation can be based on using the vertical loads due to gravity only (service loads), which in fact are the average loads applied to the posts during the actual cyclic (seismic) loading history.

Consequently, the proposed procedure can be summarised as follows:

1. Preliminary elastic analysis of the TF structure to estimate the axial stress of the timber posts due to gravity loading.
2. Discretization of the TF structure into panels consisting of two timber beams, two timber posts and a pair of timber diagonal braces.
3. NL analysis of the TF panels under horizontal loading using the complex model.
4. Generation of pushover curves for the TF panels.
5. Transformation of the pushover curve into a simple bilinear one and definition of the yield (V_y - δ_y) and failure (V_u - δ_u) points. This transformation is done here using the familiar equal energy absorption rule (equal areas between the bilinear and the original curves), but other valid procedures could also be used.
6. Modification of the axial stiffness of the diagonals to take into account their expected sliding. The following relationship can be used (Kouris and Kappos 2012):

$$k_s = \frac{(H^2 + L^2)^{3/2} + H^3}{EA} \cdot \frac{1}{L^2} \cdot \frac{V_y}{\delta_y} \quad (5)$$

where H and L are the height and the length of the panel, E is the modulus of elasticity for wood, and A is the area of the timber brace section. The modified elastic axial stiffness of the diagonals K_{el} should be calculated as follows:

$$E' = k_s E \quad (6a)$$

$$K_{el} = E' A / L \quad (6b)$$

Using the secant axial stiffness of the diagonals the axial deformation at yield can be calculated from the following equation:

$$u_{diag,y} = N_{diag,y} / K_{el} \quad (7)$$

7. Determination of the NL law of the axial hinges according to the following relationships:

$$N_{diag} = V \frac{\sqrt{H^2 + L^2}}{L}, \quad \mu_d = \frac{\delta_u}{\delta_y} = \frac{u_{diag,u}}{u_{diag,y}} \quad (8)$$

8. Insertion of plastic hinges in the diagonals of the model, which can carry compressive loads only.
9. NL static analysis to determine the pushover curve of the structure.

The proposed procedure was applied to the specimens tested at IST. Steps 1 to 5 result in the bilinear curves of Figure 18. The final deformed shape of the model is shown in Figure 19 where the plastic hinge state is illustrated with red colour for failure and yellow for close to failure. The

derived pushover curve is plotted in Figure 20 against the experimentally derived hysteresis loops. Both displacements and base shears are in fairly good agreement with the envelope of the experimental results. The difference in maximum base shear is 8.9% for specimen SC2 and 17.5% for specimen SC3. However, it should be pointed out that at the maximum drift these differences are much lower (less than 10%) and for a model aiming to capture the overall response by an almost bilinear curve it is sufficient just to target at an 'equivalent' base shear.

The modification factors k_s of step 6 are calculated according to Equation 6 and values 0.09, 0.25, 0.10 and 0.19 are found for panels 1 to 4, respectively.

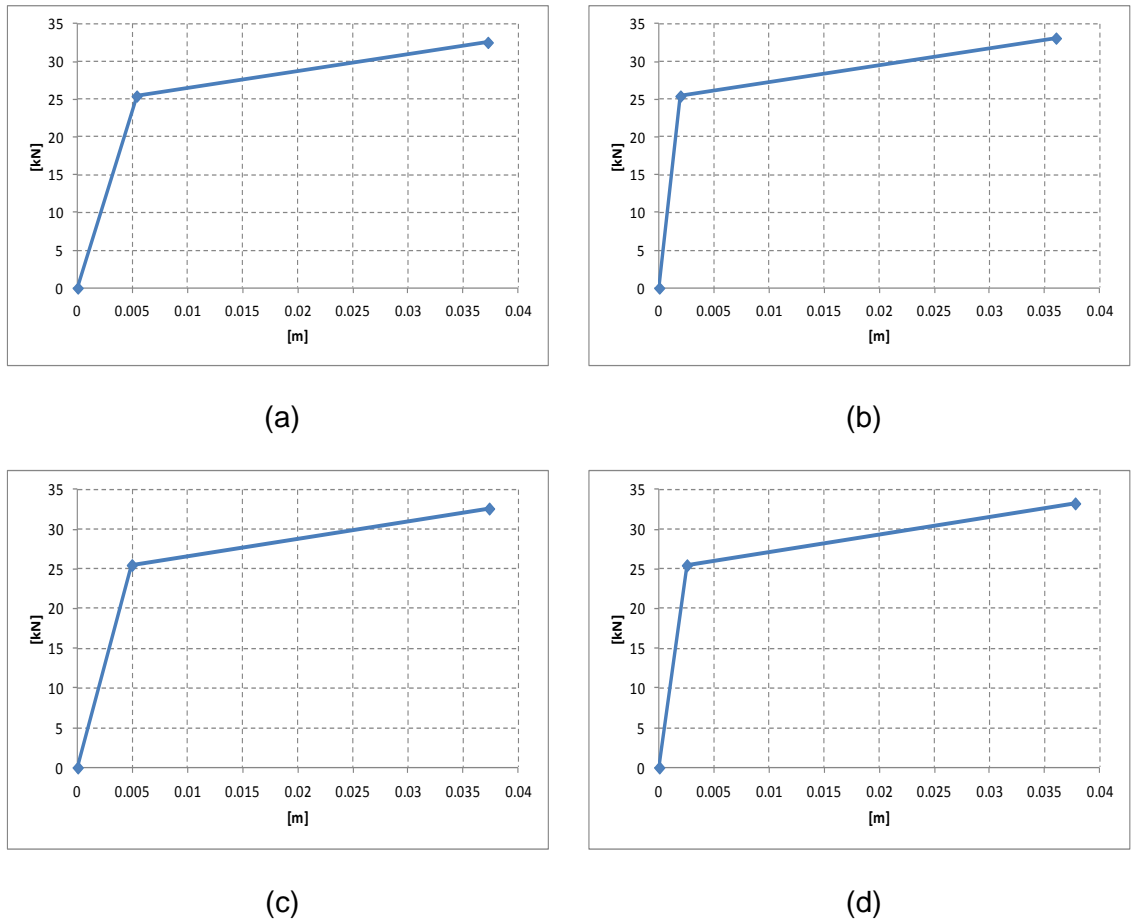


Figure 18 Bilinear curves of the pushover curves of the four TF panels of IST laboratory (a to d correspond to panels 1 to 4, respectively).

The final deformed shape of the model is shown in Figure 19 where the plastic hinge state is illustrated with red colour for failure and yellow for close to failure. The derived pushover curve is plotted in Figure 20 against the experimentally derived hysteresis loops. Both displacements and base shears are in fairly good agreement with the envelope of the experimental results. The difference in maximum base shear is 8.9% for specimen SC2 and 17.5% for specimen SC3. However, it should be pointed out that at the maximum drift these differences are much lower

(less than 10%) and for a model aiming to capture the overall response by an almost bilinear curve it is sufficient just to target at an 'equivalent' base shear.

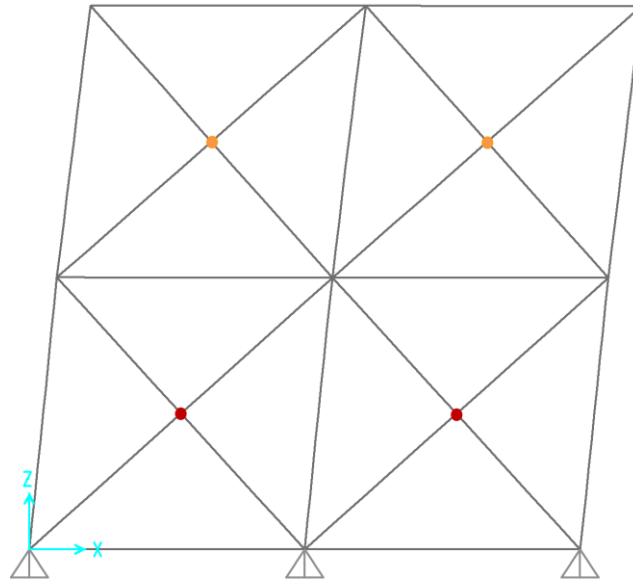


Figure 19 Deformation of the TF panel at its final step of analysis: red bullets imply failure and orange bullets imply close to failure.

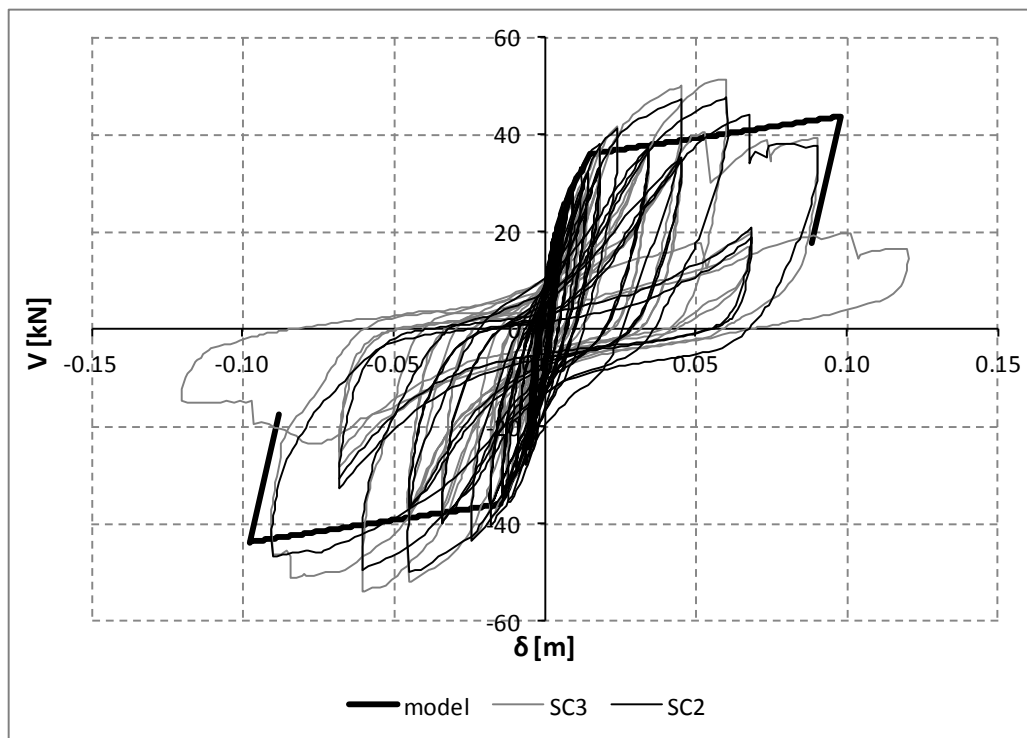


Figure 20 Pushover curve from the model versus experimental hysteretic loops (IST tests).

Displacements of the analytical model are in good agreement with specimen SC2. However, SC3 has an ultimate displacement 20% higher than that of the analytical model, but for a

hysteresis loop with significant stiffness and strength degradation; on the contrary, the last cycle of almost constant strength is very close to the analytical model. Moreover, the initial stiffness is well captured. The comparison with specimen SC1 leads to similar conclusions.

4.2. Empirical model based on IST tests

The phenomenological hysteresis model presented herein was developed by Meireles et al. (2011, 2012). In the present study that focuses on NL static analysis, only envelope curves are considered and comparison between experimental and analytical curves is carried out in terms of envelopes.

The hysteresis model was developed based on a minimum number of path-following rules that can reproduce the response of the wall tested under general monotonic or cyclic loading. It was constructed using a series of exponential and linear functions and calibrated according to the experimental tests on the 2x2 panels (see section 2). Figure 21 illustrates the basic features of the hysteresis model for TF walls.

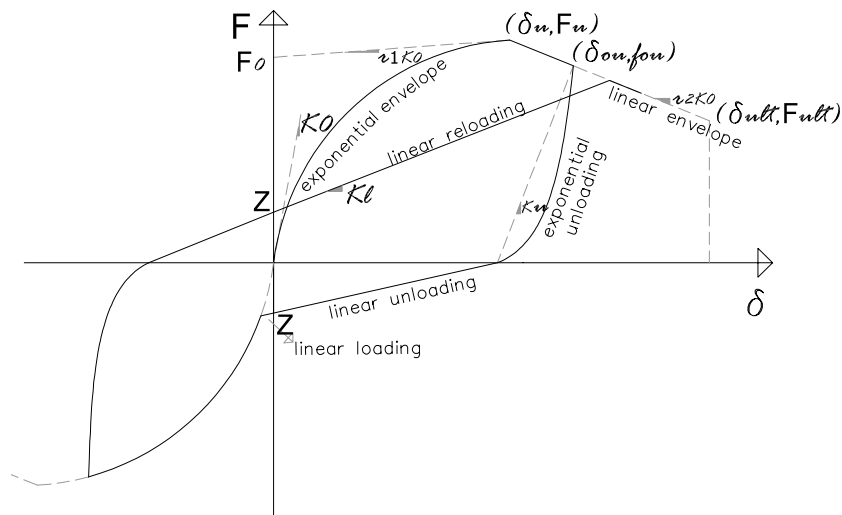


Figure 21 Phenomenological hysteresis model.

The envelope curve is modelled using one exponential and one linear function, as shown in Fig. 21. The exponential function defines the ascending branch (*exponential envelope*) and the linear function the descending branch (*linear envelope*). The envelope curve is defined by 6 identifiable parameters that were fitted to experimental data. The parameters, illustrated in Figure 21, are F_0 , K_0 , r_1 , r_2 , δ_u and δ_{ult} . The force-displacement relationships are defined, by these parameters - equation (9).

$$F = \begin{cases} (F_0 + r_1 K_0 \delta) \cdot (1 - e^{(-K_0 / F_0 \delta)}) & \text{for } \delta \leq \delta_u \quad (a) \\ F_u + r_2 K_0 (\delta - \delta_u) & \text{for } \delta_u < \delta \leq \delta_{ult} \quad (b) \\ 0 & \text{for } \delta > \delta_{ult} \quad (c) \end{cases} \quad (9)$$

The exponential function used to describe the ascending branch (Equation 9a) was first proposed by Foschi (1974) and later used by Folz and Filiatrault (2001) to model the response of wood shear walls. Beyond the displacement δ_u , which corresponds to the ultimate load F_u , the load-carrying capacity is reduced. Failure of the wall under monotonic loading occurs at displacement δ_{ult} . It has been assumed that the wall's monotonic deformation capacity corresponds to a drop in strength equal to 20% of the maximum (ultimate) load F_u or when a maximum drift of 3.5% is reached. In this case, δ_{ult} is already defined based on r_2 , δ_u and F_u ; hence, the number of identifiable parameters is reduced to 5.

Figure 22 shows the comparison between the envelope curves developed by the previously described model and the results of the experimental testing (2x2 panel); it is seen that the model's envelope curves were well fitted to the experimental results. In this case, the black curves are terminated at the assumed failure of the wall, based on the 20% drop in strength criterion.

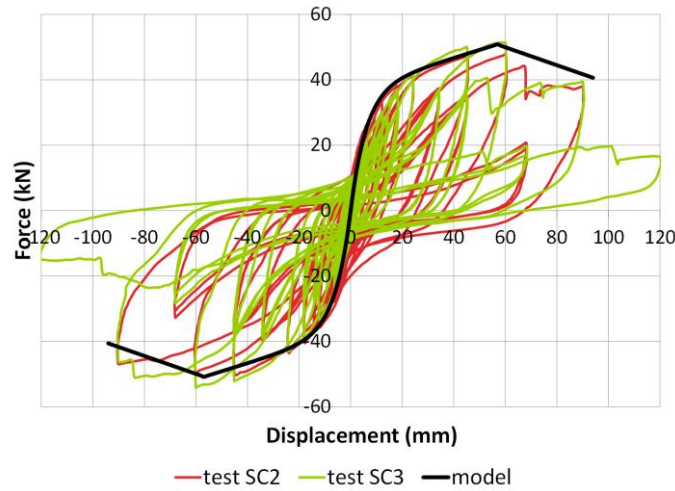


Figure 22 Phenomenological model applied to the IST test results.

4.2.1. Calibrating the 2x2 panel based on the experimental initial stiffness, K_0

An analytical model of the wall was set up in SAP 2000 (1998) in order to predict its behaviour in the linear range (i.e. to predict the initial stiffness, K_0). In this way, the model was calibrated according to the initial stiffness obtained. The analytical model developed (Figure 23) has the following properties:

- The diagonals of the wall resist compression only, as also found by Cardoso et al. (2005) and Meireles (2012).
- Shell elements were used to model the masonry.

- c) Pinned connections were used at the nodes; this is not fully representative of nailed connections, but is more practical for a macro - scale modelling approach.
- d) Rigid links were adopted to connect the shell elements of the masonry to the diagonals in order to simulate the thickness of the diagonals and the true area of the masonry, implying a 100% load transfer.
- e) At the supports, springs were used to simulate the effect of rigid body movement (discussed later in this section).
- f) Vertical loads applied matched the ones from the experimental testing.

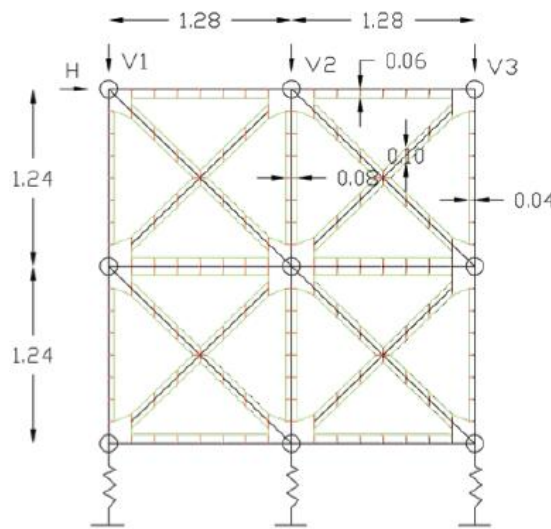


Figure 23 Analytical model for estimating initial stiffness (units in m).

In Figure 23, the green lines define the areas of the masonry shell elements; the red lines define the rigid links, and the black lines define the timber elements. In the same figure, H is the applied horizontal force and V1, V2 and V3 are the vertical forces in the posts. The springs at the supports model the effect of rigid body movement observed during the tests. More specifically, the nailed connections at the bottom are moving upwards and downwards and this gives rise to a rigid body movement of the specimen. Note that the bottom horizontal timber beam is tightly fixed to the horizontal steel reaction beam of the testing rig, so the rigid body movement only comes from the displacement of the nailed connections. The springs are calibrated for the model to match the initial experimental stiffness of the tested walls. It is noted that one could assume that the calibrated spring stiffness is the same regardless of the panel configuration, i.e., the same one for a 2x2 or 3x2 panel pattern, since the spring represents a nailed connection and these are the same for all the panels. It is also assumed that the compression stiffness of the springs is the same as the tension stiffness, in the absence of more specific evidence.

The mechanical properties of wood and masonry assumed for the model are described in the following. Properties of wood were taken from LNEC norm for *Pinho Bravo para estruturas* (LNEC 1997) based on several mechanical tests made on the Portuguese *Pinus Pinaster* (the

wood used in the tests). Based on this work, the Young's Modulus of elasticity is 12,000 MPa, the density 580 kg/m³ and the Poisson's ratio 0.2. With respect to masonry, Carvalho (2007) has carried out some testing on hydraulic mortar with the same characteristics as the mortar used in the IST test presented (2x2 panels). The value used for the Modulus of elasticity of masonry was 770 MPa, the density 22 kN/m³, this time, and Poisson's ratio 0.2, based on the Portuguese Technical Tables (1998). To derive the appropriate spring stiffness, 3 spring stiffnesses were explored: 6,000, 10,000 and 15,000 kN/m. Table 3 shows the results obtained, aiming to find the optimal spring stiffness. In this table K_{anal} is the analytical estimation of initial stiffness and K_0 is the experimental value of initial stiffness. It can be seen in the table that the spring stiffness that makes the model have an initial stiffness equal to the experimentally obtained stiffness is $K_{spring}=15,000$ kN/m. This is the spring stiffness used for the subsequent configurations studied in the next section.

Table 3. Ratio of analytical over experimental stiffness for different spring constants.

V1, V3 (kN)	V2 (kN)	H (kN)	K_{spring} (kN/m)	Top horiz. displ. (mm)	K_{anal} (kN/mm)	K_{anal}/K_0
19.2	38.4	30	6000	10.3	2.9	0.5
19.2	38.4	30	10000	6.5	4.6	0.8
19.2	38.4	30	15000	4.6	6.4	1.0

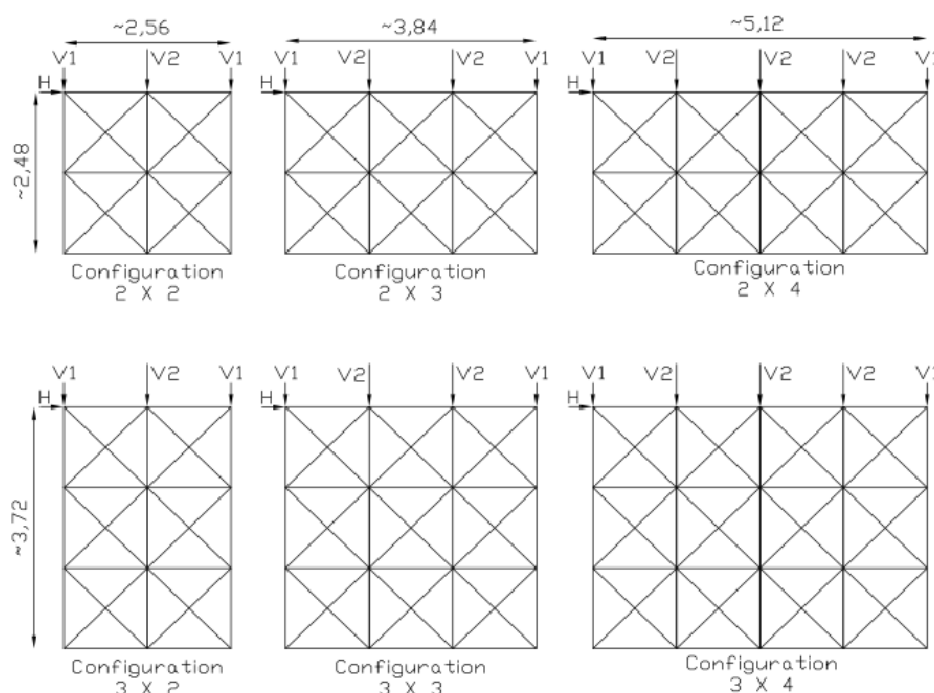


Figure 24 Configurations of TF walls studied.

4.2.2 Predicting the initial stiffness for other configuration of walls

The main purpose of this section is to estimate the initial stiffness for other configurations of walls. Figure 24 shows the configurations of walls studied. These configurations are common in *Pombalino* buildings.

The 2x2 configuration is the one tested at IST; the 3x2 configuration was tested at LNEC (Santos 1997). The others are possible existing configurations. Table 4 shows the values obtained analytically (K_{anal}) for the initial stiffness of the different configurations of walls. In this study it was again assumed $E_{wood}=12,000$ MPa, $E_{masonry}=770$ MPa, and the horizontal force applied (H) was 30 kN, the vertical load (V1) was 19.2 kN and V2 was 38.4 kN. The structural/analytical models for all configurations are similar to the previously presented model for configuration 2x2. One can also see that, as expected, configuration 3x2 is the one with the lowest stiffness while configuration 2x4 is the one with the highest stiffness. Also, within each set (number of storeys) the stiffness increases, as anticipated, as the aspect ratio (height/length) decreases.

Table 4. Initial stiffness for different configurations of walls

Model Configuration	Top horiz. displ. (mm)	K_{anal} (kN/mm)	Aspect ratio (height/length)
2x2	4.6	6.4	0.97
2x3	1.9	15.8	0.65
2x4	0.9	33.3	0.48
3x2	10.3	2.9	1.45
3x3	4.4	6.8	0.97
3x4	2.2	13.6	0.72

4.2.3 Estimating the strength of the panel for all configurations

The failure mode of the wall was buckling and further cracking of one of the diagonals and later others. Figure 25 shows this failure mode. In view of this, the strength of the panel can be associated to the collapse of the most loaded diagonal.



Figure 25 Buckling and cracking of diagonal.

At this stage, the compression force on the most loaded diagonal of the tested configuration 2x2 was estimated. The idea is to estimate the strength associated with failure of the most loaded diagonal on other wall configurations (Figure 24). The structural models developed in SAP 2000 (1998) for determining the most loaded diagonal are simple trusses with springs at the bottom and pinned connections at member ends (Figure 26). In this way, the contribution of the masonry infill is neglected. At the development of (ultimate) strength, masonry is extensively detached from the truss elements and considerably cracked at some locations, as has been discussed in Meireles (2012) and Kouris and Kappos (2012). The stiffness of the springs is the same as previously estimated. The compression force (strength) on the most loaded diagonal of the tested 2x2 configuration was 49 kN. This value is the force at the most loaded diagonal when the structure attains its strength F_u . It is then required to estimate the value of F_u for other wall configurations. It is assumed that, when the most loaded diagonal in a structure with another configuration reaches the value -49 kN it then fails by buckling. In this way, one can calculate the horizontal force, F_u , associated with each configuration. Table 5 shows the values of F_u obtained for the other configurations.

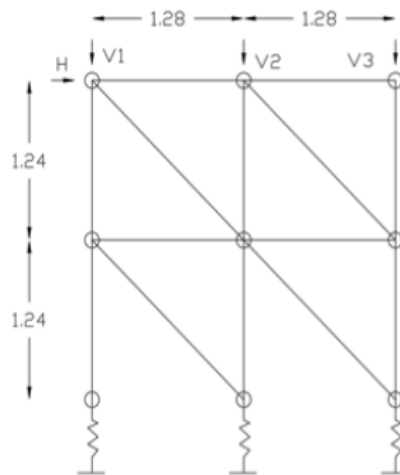


Figure 26 Model adopted for estimating strength (dimensions in m).

According to the values reached the configuration with the highest strength (F_u) is the 2x4 one, followed by the 3x4 configuration. The configuration with the lowest strength is 3x2. The diagonals reaching 49 kN are the bottom right diagonals if force is applied from left to right.

Table 5. Calculation of F_u for different wall configurations

Configuration	F_u (kN)
2x3	72.4
2x4	111.6
3x2	49.9
3x3	68.6
3x4	90.0

4.2.4 Prediction of envelope curves for other wall configurations

The envelope curve determined for other wall configurations is based on the following assumptions:

- The initial stiffness, K_0 , is taken from the analysis carried out for each wall configuration.
- The value of F_{ult} , which is the strength attained by the wall, was determined previously for each wall based on the assumptions presented in 4.2.3 and the wall configuration.
- The value of $r_1 K_0$, $r_2 K_0$ and $\zeta (=F_0/F_u)$ are constant for all wall configurations and taken as the experimental values obtained for the tested 2x2 configuration.
- The value of F_{ult} (denotes failure) was defined when one of following conditions was reached: 1) the strength drops to 80% of F_u or 2) a drift of 3.5% is reached. It is worth mentioning that in both experimental tests summarised in section 2 the panels failed at a drift of about 3.5%, which is quite higher than that associated with failure of unreinforced masonry structures. According to the drift criterion, configurations C2x2, C2x3, C2x4 have ultimate displacements of about 90 mm, while configurations C3x2, C3x3, C3x4 have values of about 120 mm.

Figure 27 depicts the envelope curves for different configurations of walls and their relative performance with respect to the analytically obtained envelope curve for the tested configuration (2x2). It can be seen that the configuration with both highest stiffness and highest strength is C2x4; the configuration with the lowest stiffness and lowest strength is C3x2.

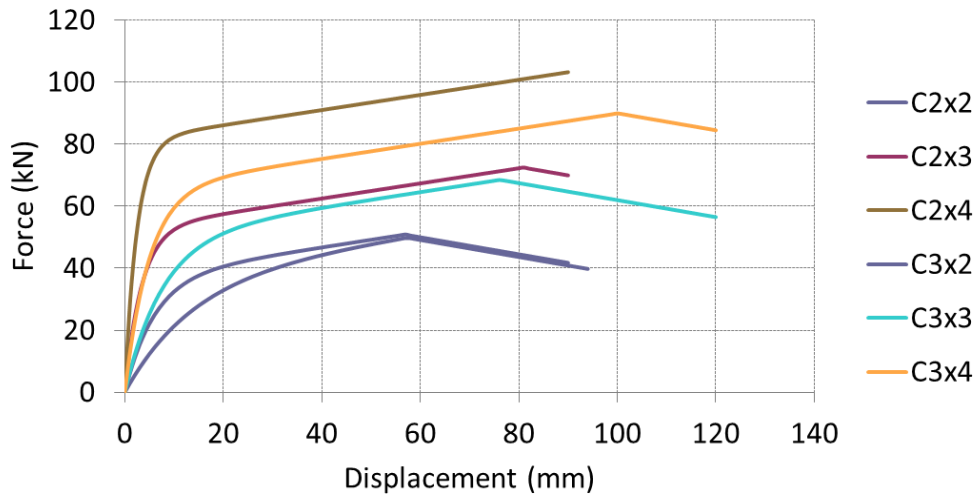


Figure 27 Various envelope curves for different wall configurations.

4.2.5. Comparison with the LNEC tests (3x2 panel)

Since the phenomenological model was calibrated on the basis of the IST tests it is important for its verification to test it in the light of an independent experimental programme. Hence, in this section, the simple model proposed and presented previously for the configuration C3x2 is used

and results are compared with the LNEC experimental envelopes. The comparison is shown in Figure 28. It can be seen that the prediction is quite reasonable given also the dispersion in the results of the LNEC testing. The simple model slightly underpredicts the strength of G1 and G2, but predicts quite well that of G3.

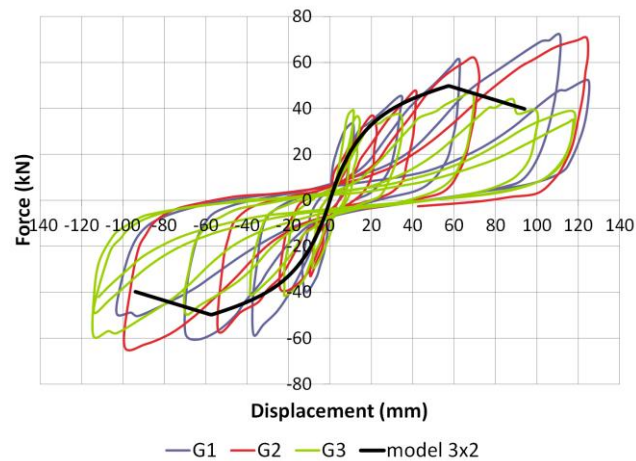


Figure 28 LNEC hysteresis vs. envelope curve prediction.

Conclusions

A comparative assessment of one complex and two simple models for pushover analysis of timber-framed masonry walls with diagonal braces has been made, in the light of available test results from two experimental programmes. The simple (macroscopic) and complex (microscopic) analytical models were used to predict pushover curves that were compared with the envelope curves of the experimental hysteresis loops. The main advantages and disadvantages of the models are summarised in Table 6 and briefly discussed in the following. It should be noted here that, as with most models, those reported herein are strictly applicable to TF walls with comparable connections, boundary conditions, infill masonry, and workmanship.

The (plasticity-based) micro - model of Kouris and Kappos (2012), which was further verified here by including the effect of the masonry infill, was found to compare well with the experimental results, offering good predictions in terms of both base shear and displacement. The model can also provide predictions of other, local, quantities, like penetration of one member into another, or relative sliding between members. Nevertheless, the main advantage of this rather complex model is its versatility, i.e. that it can be applied to virtually any TF wall configuration, since it does not include parameters that are calibrated on the basis of test results.

Then two relatively simple approaches were evaluated, intended for the NL static analysis of realistic buildings. The first one, involving familiar beam-column elements, is directly connected to the complex model, since it treats the individual TF panels as substructures, and the nonlinear behaviour of each panel is estimated with the aid of the micro - model. The procedure

is developed in nine steps and was found to lead to a reliable estimate of the pushover curve of the tested specimens with a reduced computational effort; the accuracy is slightly lower than that of the complex model, still quite acceptable for all practical purposes. Although it is feasible to analyse relatively large structures using this approach (especially suitable if several panels are identical and hence have to be analysed only once with the complex model), it is clear that it is practically important to make this model self-standing, i.e. not requiring the use of the complex models for the substructures; a first attempt in this direction has been made by Kouris (2012).

The second simple approach is a phenomenological one wherein the basic parameters for the envelope curve of the hysteresis loops were identified on the basis of the IST test results. The model was used here for wall configurations other than the tested 2x2 panel and comparisons were made with other tests (LNEC), not used for its calibration. Although the prediction of key parameters such as strength was a bit inferior to that from the other (more time-consuming) models, they are acceptable for practical purposes. Moreover, unlike the previous models, this simple model has the capability to simulate response under cyclic loading, an issue not specifically addressed herein, but crucial in seismic assessment of structures.

In Table 6 a 'pseudo-quantitative evaluation is made of all models presented herein. It is noted that with regard to versatility the evaluation refers to the practicality and ease of use, while with regard to calibration it refers to a self-standing procedure, i.e. no need for additional calibration against experimental results.

Table 6. Comparative summary of the models used in the present study

	calibration	accuracy	versatility
Micro - model	***	***	*
Macro - model A (substructure)	**	**	***
Macro - model B (phenomenological)	**	**	**

Note: The number of stars reflects the suitability of each model with regard to the particular aspect considered.

Acknowledgements

The author H. Meireles would like to acknowledge the financial support of the Portuguese Foundation for Science and Technology (Ministry of Science and Technology of Portugal) through the research project PTDC/ECM/100872/2008 and through the PhD scholarship SFRH/BD/41710/2007. The author L. Kouris acknowledges the financial support provided by the 'Bodossaki Foundation' (Athens, Greece) for carrying out his PhD work.

References

- ANSYS User's Manual, Revision 13.0, Swanson Analysis Systems, Inc., Houston, PA, 2011.
- Addessi D, Marfia S, Sacco E (2002) A plastic nonlocal damage model. *Comput Methods Appl Mech Eng* 191: 1291-1310
- Cardoso R, Lopes M, Bento R (2005) Seismic Evaluation of Old Masonry Buildings. Part 1: Method Description and Application to a Case-Study. *Engineering Structures*, 27: 2024-2035
- Carvalho J (2007) Caracterização Mecânica de Paredes Resistentes em Alvenaria de Pedra através de ensaios não destrutivos; [Mechanical characterization of stone masonry walls through non-destructive tests] Master Thesis, IST (*in Portuguese*).
- Cruz H, Nunes L, Machado JS (1998) Update assessment of Portuguese maritime pine timber. *For Prod J* 48: 60-64
- Doudoumis IN (2010) Analytical Modelling of Traditional Composite Timber-Masonry Walls. *Advanced Materials Research*, 133: 441-446
- Drucker DC, Prager W (1952) Soil mechanics and plastic analysis or limit design. *Q Appl Math* 10: 157-165
- Folz B, Filiatrault A (2001) Cyclic analysis of wood shear walls. *J Struct Eng (ASCE)* 127(4): 433–441.
- Foschi RO (1974) Load-slip characteristics of nails. *Wood Sci* 7(1): 69–76.
- Hill R (1948) A Theory of the Yielding and Plastic Flow of Anisotropic Metals. *Proceedings of the Royal Society of London, Series A, Mathematical and Physical Sciences* (1934-1990) 193: 281-297.
- Krawinkler, H, Parisi F, Ibarra L, Ayoub A. and Medina R (2000) Development of a testing protocol for wood frame structures. CUREE-Caltech Wood frame Project Rep., Stanford University, Stanford, California.
- Kouris LAS (2012) Seismic assessment of timber-framed masonry buildings. PhD thesis, Aristotle University of Thessaloniki, Dept. of Civil Engineering (*in Greek*).
- Kouris LAS, Kappos AJ (2012) Detailed and simplified non-linear models for timber-framed masonry structures. *J Cult Heritage* 13(1): 47-58
- Lourenc o PB (2000) Anisotropic softening model for masonry plates and shells. *J Struct Eng ASCE* 126(9): 1008-1016.
- Lourenc o PB, De Borst R, Rots JG (1997) A plane stress softening plasticity model for orthotropic materials. *Int J Numer Methods Eng* 40: 4033-4057.
- Mascarenhas J, (2005) Sistemas de Construc  o V-O Edif  cio de rendimento da Baixa Pombalina de Lisboa, *Materiais B  sicos 3  Parte: O Vidro*. [Construction Systems V- The building stock of Lisbon downtown, Basic materials 3rd part: Glass] *Livros Horizonte (in Portuguese)*.
- Meireles H, Bento R, Cattari S, Lagomarsino S (2012) A hysteretic model for “frontal” walls in *Pombalino* buildings. *Bull Earthquake Eng* 10:1481–1502.

- Meireles H, Bento R, Cattari S, Lagomarsino S (2011) The proposal of a hysteretic model for internal wooden walls in *Pombalino* buildings, Proceedings of the World Congress on Advances in Structural Engineering and Mechanics (ASEM11plus), Seoul, South Korea.
- Meireles H (2012) Seismic Vulnerability of Pombalino Buildings. PhD Dissertation, IST Technical University of Lisbon.
- Page AW (1981) Biaxial compressive strength of brick masonry. *Proc Inst Civ Eng (London)* 71: 893-906
- Pallarés FJ, Aguero A, Ivorra S (2008) A comparison of different failure criteria in a numerical seismic assessment of an industrial brickwork chimney. *Mater Struct* 1-14.
- Parisi MA, Piazza M (2000) Mechanics of plain and retrofitted traditional timber connections. *J Struct Eng (ASCE)* 126: 1395-1403.
- Patton-Mallory M, Pellicane PJ, Smith FW (1997) Modeling bolted connections in wood: review. *J Struct Eng (ASCE)* 123: 1054-1062.
- Pinho Bravo para estruturas (1997) Madeira para construção [Structural Timber], M2, LNEC (*in Portuguese*).
- Santos PS (1997) Laboratory tests on masonry walls taken from an ancient building in Lisbon. 17/97, Lisbon, Portugal.
- SAP 2000 (1998) Three Dimensional static and dynamic finite element analysis and design of structures, version 7.4.2, CSI, computers and structures, inc, Structural and Earthquake engineering software, Berkeley, California, USA.
- Shih CF, Lee D (1978) Further developments in anisotropic plasticity. *J Eng Mater Technol Trans ASME* 100: 294-302
- Syrmakezis CA, Asteris PG (2001) Masonry failure criterion under biaxial stress state. *J Mater Civ Eng(ASCE)* 13(1):58-64
- Technical Tables (1998) Brazão Farinha JS, Correia dos Reis A, Edições Técnicas E.T.L. Lda (*in Portuguese*).